Modeling spark plasma sintering of zirconia with prediction of final stage high densification rate

Joseph Sambasene Diatta, Christophe Couder, Christelle Harnois, Sylvain Marinel, Charles Manière

Modeling spark plasma sintering of zirconia with prediction of final stage high densification rate

Joseph Sambasene Diatta[1*], Christophe Couder[2], Christelle Harnois[2],
Sylvain Marinel[2], Charles Manière[2*]

1 Assane Seck University, Ziguinchor, Sénégal

2 Normandie Univ, ENSICAEN, UNICAEN, CNRS, CRISMAT, 14000 Caen, France

* charles.maniere@ensicaen.fr ; jsdiatta@univ-zig.sn

Keywords: Spark Plasma Sintering, final stage sintering, zirconia, modeling,

Abstract:

In this study, the SPS ~~sintering~~ of 0.1µm zirconia has been performed and shows high densification rate behavior in the final stage. This work consists of modeling the densification behavior of this powder especially at the intermediate/final stage transition. To model this, a Master Sintering Curve (MSC) is combined with an analytic model to identify the activation energy and the sintering moduli. The modeling of the behavior of the powder during the sintering tests is done *via* the Skorohod-Olevsky model. It appears from this study that the modeling of final stage sintering requires a regime transition to model the exceptionally high densification rate of the powder. The final stage grain growth seems not to decrease the final stage sintering kinetics.

Nomenclature

θ Porosity
ρ Relative density
σ_z Applied stress ($N.m^{-2}$)
H A constant
D Diffusion coefficient ($m^2.S^{-1}$)
k Boltzmann Constant ($1.380\ 649 \times 10^{-23}\ J.K^{-1}$)
ϕ Stress intensification factor
G Grain size (m)
n Creep law stress exponent
m Creep law grain size exponent
A Creep deformability ($s^{-1}Pa^{-n}$)

A_0 Creep coefficient ($Ks^{-1}Pa^{-n}$)

Q Creep activation energy ($J.mol^{-1}$)

R Gas constant 8.314 ($J.mol^{-1}.K^{-1}$)

T Temperature (K)

φ Shear modulus

ψ Bulk modulus

P_l Sintering stress (Pa)

α Surface energy ($J.m^{-2}$)

r Particles radius (m)

a, b, μ Fitting constants

θ_c Critical porosity

I. Introduction

Sintering modeling of processes like the spark plasma sintering (SPS) represents a key step for optimizing the thermal/pressure cycle optimization and also to be able to simulate the powder densification in finite element software (FEM)[1]. The continuum theory of sintering can be employed to simulate the SPS ~~sintering~~ analytically and identify sintering parameters easily implementable in FEM code[2]. Hot pressing (and SPS) solid-state sintering model is expressed after.

$$\frac{1}{\rho}\frac{d\rho}{dt} = \frac{HD(T)\phi(\rho)^n\sigma_z^n}{G^m kT} \quad (1)$$

This model generally assumes the applied stress is higher than the capillarity stress ($\sigma_z \gg Pl$). However, if the powder is submicronic these forces are not negligible and should be taken into account $\sigma_z^n \rightarrow (\sigma_z - P_l)^n$. Skorohod sintering stress expression is taken as it gives a reasonable approximation when compared to other theories[3,4], $P_l = \frac{3\alpha(1-\theta)^2}{r}$. If the Skorohod-Olevsky continuum model[2] is employed, the temperature dependent term is $A(T,G) = \frac{HD(T)}{G^m kT} = \left(\frac{G_0}{G}\right)^m A_0 exp\left(\frac{-Q}{RT}\right)$ and the stress intensification factor ($\phi(\rho)$) depends on shear φ and bulk ψ moduli porosity functions that can be approximated theoretically[5] $\phi = \left(\left(\psi + \frac{2}{3}\varphi\right)^{\frac{-n-1}{2}}(1-\theta)^{\frac{1-n}{2}}\right)^{\frac{1}{n}}$. The assessment of the sintering parameters requires to identify first the thermal behavior A(T,G) in a high porosity region where the grain growth is inactive. To do so, the master sintering curve or kinetic field methods that can be adapted to SPS equations can be done to identify independently the sintering activation energy[6,7]. With this

information, the theoretical moduli can be adjusted by a linear regression equation and other parameters determined. This approach has been used for conventional sintering of zirconia[8], $MgAl_2O_4$ spinel[9] and requires less sintering tests than the full extensive approaches that identify both creep and moduli[10–14].

In this study the combined master sintering curve and moduli adjustment method is adapted to SPS of submicronic zirconia.

II. Materials and Method

The study has been performed with SPS FCT HP25 device and with a binderless 0.1µm Tosoh TZ-3Y-S zirconia powder. For the master sintering curve (MSC) and the simulation analysis study three sintering tests at 20, 50 and 100K/min have been performed at 50MPa of pressure up to 1350°C.

The sintering assessment method consists of three steps. Step 1 is the independent determination of the sintering activation energy (*via* the MSC) by finding the activation energy that minimizes the three tests curves differences when plotting the relative density *vs* $ln(\int_0^t \frac{exp\left(\frac{-Q}{RT}\right)}{T} dt)$ [15].

For step 2, the following Skorohod-Olevsky analytical SPS equation is used:

$$-\frac{1}{\rho}\frac{d\rho}{dt} = A(T,G)\left(\psi + \frac{2}{3}\varphi\right)^{\frac{-n-1}{2}}(1-\theta)^{\frac{1-n}{2}}(\sigma_z - P_l)^n \quad (2)$$

In the latter, A(T) is isolated to obtain the regression equation giving A_0, Q in the intermediate stage.

$$Y = ln\left(T\left|\dot{\theta}\right||\sigma_z - P_l|^{-n}\left(\psi + \frac{2}{3}\varphi\right)^{\frac{n+1}{2}}(1-\theta)^{\frac{n-3}{2}}\right) = ln(A_0) - \frac{Q}{RT} \quad (3)$$

Knowing the MSC activation energy (Q) and n=2 for a previous study[13], it is then possible to adjust the unknown parameters of Skorohod[5] moduli ($\psi = a\frac{(\theta_c-\theta)^b}{\theta^c}$ & $\varphi = \left(1-\frac{\theta}{\theta_c}\right)^2$) to obtain the slope corresponding to the MSC value. These moduli calibration avoid the identified creep parameters (A_0,Q) compensate an error in the theoretical moduli. Afterward, the A_0 can be obtained by the origin the regression curve ($exp(A_0)$).

All parameters determined, step 3 is the analytic simulation of the sintering curve based on equation (2).

III. Results and Discussion

Figure1(A) shows the results of three experimental tests of SPS ~~sintering~~ at different heating rates (100K/min, 50K/min and 20K/min) until reaching a temperature of 1350 °C. These curves show the relative density used for the MSC study. As expected, we see that at the same relative density, the sintering temperatures are lower for the lower heating rates. Moreover, the final microstructures show very limited grain growth with grain sizes (130-200nm) close to the 100nm of the initial powder (see **Figure1(B)**). Final stage sintering shows a very fast densification close to the full density without the typical sigmoid shape of densification curves.

Figure1(C) shows the MSC performed on this powder in order to know its activation energy. The results of the MSC study gives an activation energy of $797\ \mathrm{kJ.mol^{-1}}$. Close values of 630 kJ/mol[16] and 673kJ/mol with n~2.1[17] were obtained for zirconia by SPS in the literature indicating a grain boundary sliding mechanism.

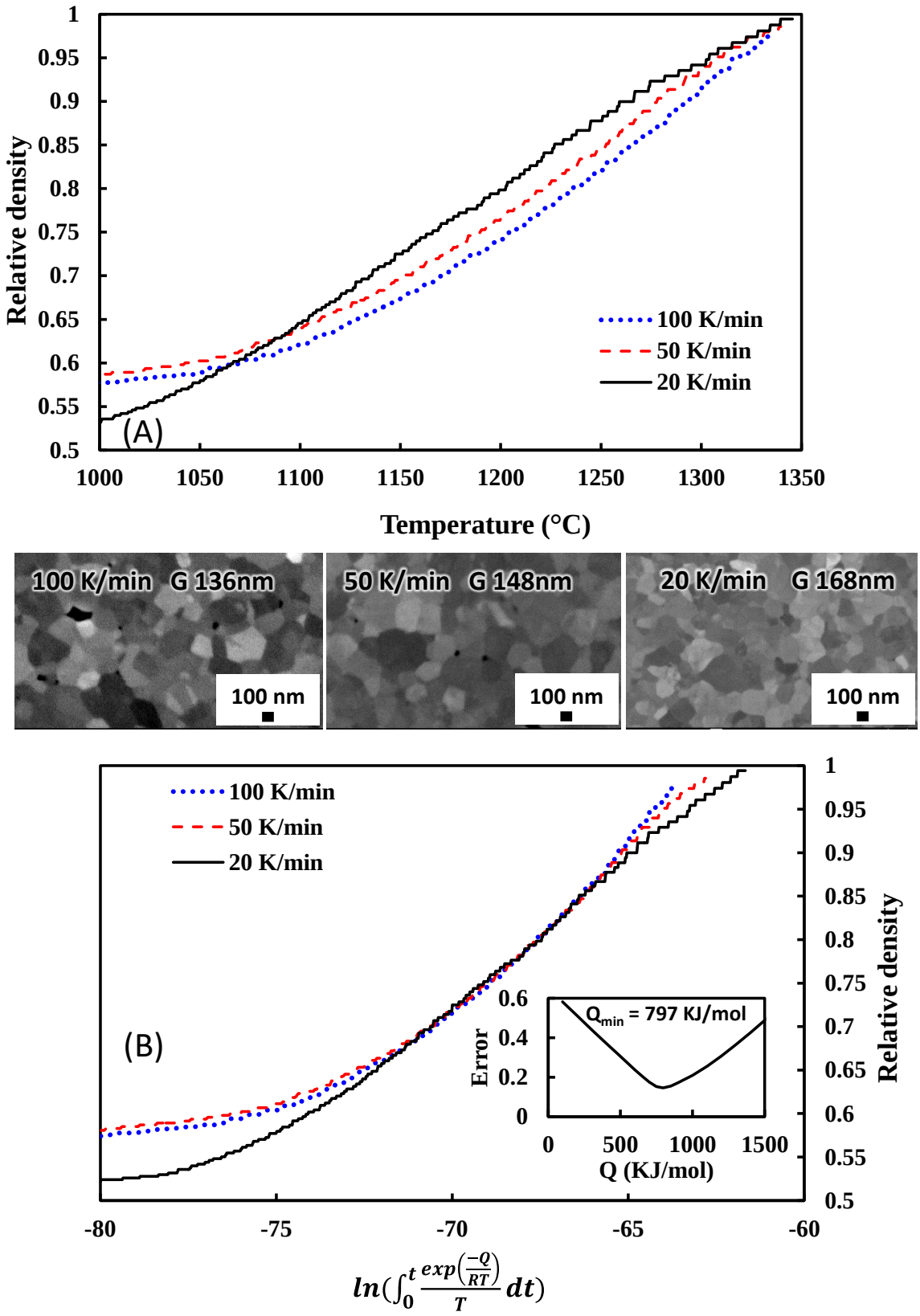

Figure 1. Relative density curves at constant heating rate of 20, 50 and 100K/min (A), polished SEM images of the final microstructures (B) and sintering activation energy identification by the Master Sintering Curve (C), in the inset is the minimization graph, the error is the distance between the curves.

As the MSC activation energy is determined by different heating rate independently from the stress intensification factor expression $\phi(\rho)$, the linear regression method described earlier can be used to correct the Skorohod moduli and determine A_0 with equation (3). **Figure2(A)** shows the results of this regression method after moduli correction. The regression for three heating rates (20, 50 and 100K/min) gives a value of the activation energy close to the MSC of $790\ \mathrm{kJ.mol^{-1}}$ and a preexponent constant A_0 of $2.16\mathrm{E}^{14}\ \mathrm{K\,s^{-1}\,Pa^{-n}}$. The corrected moduli are plotted in **Figure2(B)**. The modulus parameters are reported in **Table 1**.

$\psi = a\frac{(\theta_c - \theta)^b}{\theta^\mu}$ $\varphi = \left(1 - \frac{\theta}{\theta_c}\right)^2$	a	b	μ	θ_c
	10	3	2.8	0.51

Table 1. Coefficients of adjustment of shear and bulk viscosity moduli

In the final stage sintering, the high densification behavior observed in the curve in **Figure2(A)** makes a deviation after 1217°C. To model this, a transition switch is operated for a couple Q,A_0 of 1400kJ/mol and $1.506\mathrm{E}^{35}\ \mathrm{K\,s^{-1}\,Pa^{-n}}$ after 1217°C. This behavior is considered as a temperature-dependent regime transition (like **Figure2(A)** suggests) happening at the final stage sintering (where the sintering densification is not decreased).

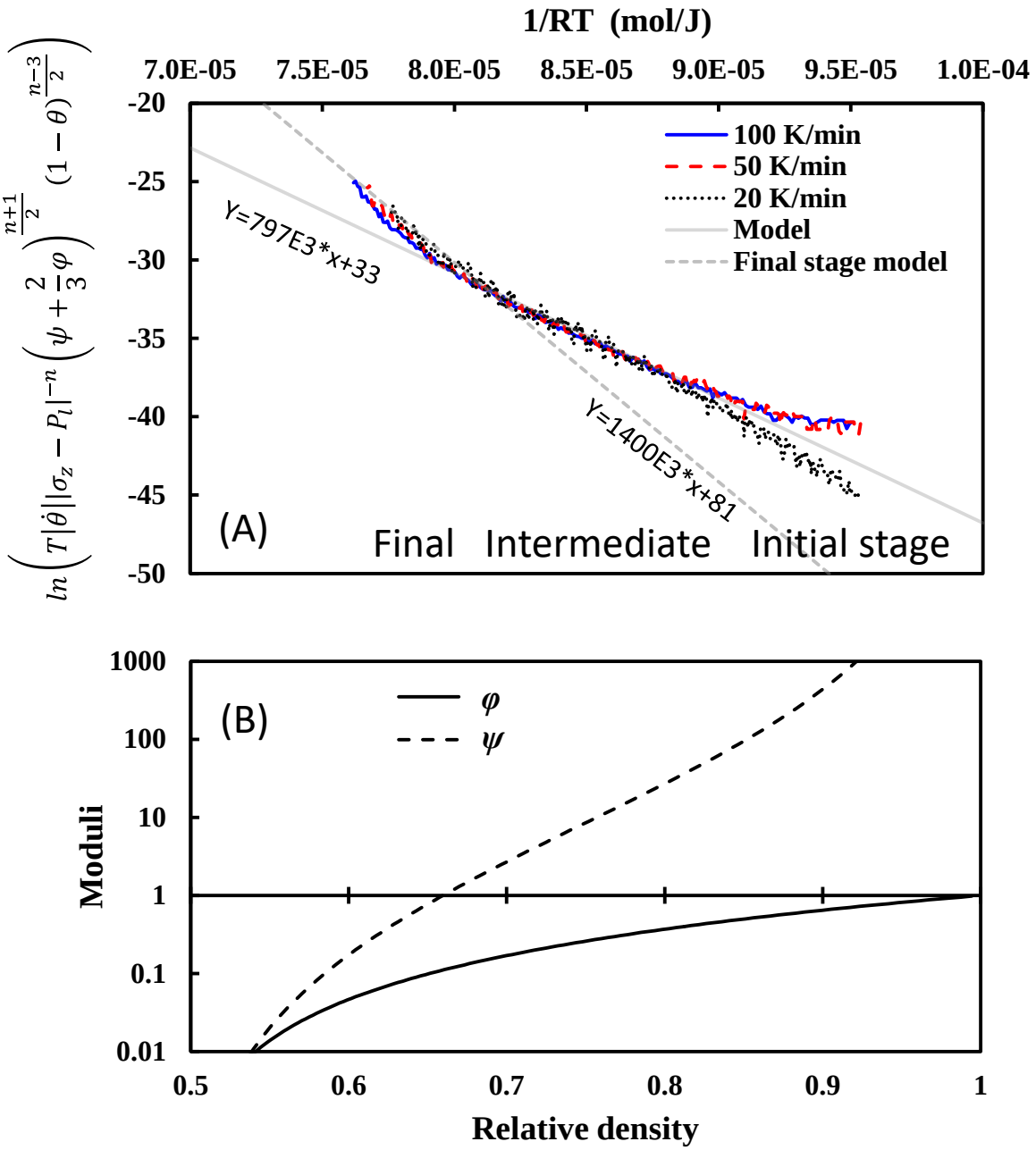

Figure 2. Regression analysis using SPS data for extraction of activation energy (A) and shear and bulk viscosity moduli as a function of time (B)

At this stage, all the sintering model parameters are identified. The modeling of the evolution of the relative density during SPS ~~sintering~~ is based on equation (2). The modeled densification curves of the powder are plotted as a function of time for the three heating rates as illustrated in **Figure3**. The simple sintering model only based on the intermediate stage parameters is compared to the comprehensive model taking into account the final stage regime transition. The densification curves clearly show that

the simple model has a typical densification kinetic decrease in the final stage. However, this typical sintering behavior underestimates the experimental relative density that have high densification kinetic at the final stage. The comprehensive model with the final stage regime transition is mandatory to simulate a realistic sintering response. This exceptionally fast sintering behavior in the final stage sintering may be explained by a combination of elements:

- Yttria partially stabilize zirconia powder was used which minimizes the grain growth that typically decreases the final stage densification kinetics.
- The powder is submicronic (0.1µm) rather than nanometric which decreases the grain growth kinetics and improve the initial powder compaction that favors final stage sintering densification without large pores.
- Finally, the SPS process favors the porosity elimination by the applied pressure and the fast kinetics that postpone surface diffusion mechanisms which help fast densification kinetics[18–20].

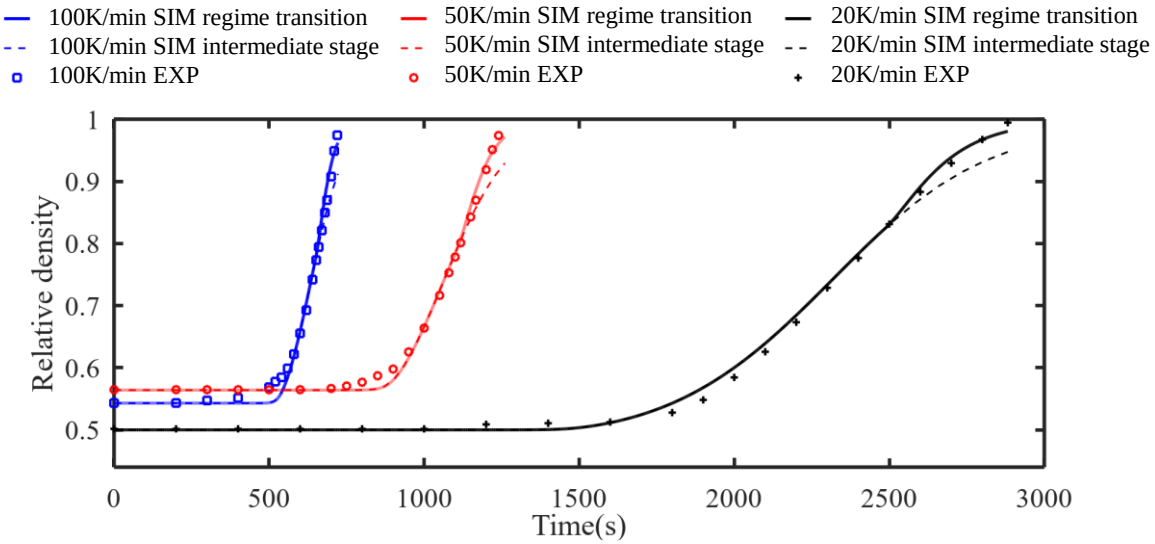

Figure 3. Simulated relative density as a function of time obtained by SPS at different heating rates, the simulation curves distinguish the identified model in “intermediate stage” without regime transition and the model including the final stage “regime transition”.

IV. Conclusion

In this study, a 0.1µm zirconia powder was sintered by SPS. Three sintering tests at 20, 50 and 100K/min were performed at 50MPa up to 1350°C. The sintering behavior shows limited grain growth and no sigmoid densification behavior at the final stage. To model this sintering behavior of the powder, the Skorohod-Olevsky model was used. A new method has been developed to identify the sintering activation energy while correcting the Skorohod theoretical moduli by coupling a regression approach and a master sintering curve. Model the experimental curves with the continuous final stage densification requires regime transition after 1217°C.

Acknowledgments

The help and support of Christelle Bilot and Jérôme Lecourt is gratefully acknowledged. This work was supported by: the French National Research Agency (ANR), project ULTRARAPIDE N°ANR-19-CE08-0033-01 and the project "région normadie" - 00016601-20E02057_RIN RECHERCHE 2020 - Emergent – ULTIMODULUS.

V. References

[1] R.K. Bordia, S.-J.L. Kang, E.A. Olevsky, J. Am. Ceram. Soc. 100 (2017) 2314–2352.

[2] E.A. Olevsky, Mater. Sci. Eng. R Reports 23 (1998) 41–100.

[3] D. Giuntini, E.A. Olevsky, J. Am. Ceram. Soc. 99 (2016) 3520–3524.

[4] F. Wakai, Y. Shinoda, T. Akatsu, Acta Mater. 52 (2004) 5621–5631.

[5] V.V. Skorohod, Nauk. Dumka, Kiev (1972).

[6] O. Guillon, J. Langer, J. Mater. Sci. 45 (2010) 5191–5195.

[7] J. Langer, M.J. Hoffmann, O. Guillon, Acta Mater. 57 (2009) 5454–5465.

[8] C. Manière, T. Grippi, S. Marinel, Mater. Today Commun. 31 (2022) 103269.

[9] G. Kerbart, C. Harnois, S. Marinel, C. Manière, Scr. Mater. 203 (2021) 114048.

[10] C. Nicolle, PhD, Mise En Forme de Poudre de Bore Par Compression Isostatique à Chaud: Determination Des Propriétés Rhéologiques et Simulation Numérique Du Procédé, Université de Bourgogne, France, 1999.

[11] C. Geindreau, D. Bouvard, P. Doremus, Eur. J. Mech. - A/Solids 18 (1999) 581–596.

[12] J. Besson, M. Abouaf, J. Am. Ceram. Soc. 75 (1992) 2165–2172.

[13] C. Manière, C. Harnois, S. Marinel, Acta Mater. 211 (2021) 116899.

[14] C. Manière, U. Kus, L. Durand, R. Mainguy, J. Huez, D. Delagnes, C. Estournès, Adv. Eng. Mater. 18 (2016) 1720–1727.

[15] H. Su, D.L. Johnson, J. Am. Ceram. Soc. 79 (1996) 3211–3217.

[16] J. Langer, M.J. Hoffmann, O. Guillon, J. Am. Ceram. Soc. 94 (2011) 24–31.

[17] A. Flaureau, A. Weibel, G. Chevallier, C. Estournès, J. Eur. Ceram. Soc. 41 (2021) 3581–3594.

[18] E.A. Olevsky, S. Kandukuri, L. Froyen, J. Appl. Phys. 102 (2007) 114913.

[19] M.-Y. Chu, M.N. Rahaman, L.C. Jonghe, R.J. Brook, J. Am. Ceram. Soc. 74 (1991) 1217–1225.

[20] X.L. Phuah, J. Jian, H. Wang, X. Wang, X. Zhang, H. Wang, Mater. Res. Lett. 9 (2021) 373–381.